frontiers | Frontiers in Marine Science

TYPE Original Research
PUBLISHED 03 August 2022
DOI 10.3389/fmars.2022.916109

OPEN ACCESS

EDITED BY
Renato Rodrigues Neto,
Federal University of Espirito Santo, Brazil

REVIEWED BY
Yifei Zhao,
Nanjing Normal University, China
Feng Liu,
Sun Yat-sen University, China
Manhua Luo,
China University of Geosciences, China
Kai Xiao,
Southern University of Science and Technology, China

*CORRESPONDENCE
Qiaona Guo
guoqiaona2010@hhu.edu.cn

SPECIALTY SECTION
This article was submitted to Coastal Ocean Processes, a section of the journal Frontiers in Marine Science

RECEIVED 08 April 2022
ACCEPTED 24 June 2022
PUBLISHED 03 August 2022

CITATION
Guo Q, Zhao Y, Li M and Liu J (2022) Radium isotope assessment of submarine groundwater discharge and associated nutrient inputs in Eastern Liaodong Bay, China. *Front. Mar. Sci.* 9:916109. doi: 10.3389/fmars.2022.916109

Radium isotope assessment of submarine groundwater discharge and associated nutrient inputs in Eastern Liaodong Bay, China

Qiaona Guo*, Yue Zhao, Mengjun Li and Jinhui Liu

School of Earth Sciences and Engineering, Hohai University, Nanjing, China

The accurate assessment of submarine groundwater discharge (SGD) and associated nutrient fluxes plays a significant role in water resources management and ecological environment protection in the coastal area. Currently, Liaodong Bay has become one of the most polluted marine areas in China. However, the nutrient fluxes carried by the SGD and its environmental effects have not yet been thoroughly reported in eastern Liaodong Bay, China. In this study, the distribution of $^{224}Ra/^{223}Ra$ activity ratio and its influencing factors under the geochemical conditions were explored. The activity of radium was affected by the water type and the geochemical factors. The radium isotopes in seawater were positively correlated with the ratios of Mg^{2+}/Na^{+} and Ca^{2+}/Na^{+} but negatively correlated with salinity and SO_4^{2-}. The average apparent water age was evaluated to be 13.0 days. Furthermore, based on the radium mass balance model, the total average SGD flux was calculated to be 1.31×10^8 m^3 day^{-1}. The nutrient fluxes carried by the SGD were 7.16×10^7, 1.01×10^6, 1.61×10^7, 0.92×10^6, and 5.41×10^7 mol day^{-1} for DIN, DIP, NH_4^+, NO_2^-, and NO_3^-, respectively. The nutrient inputs through the SGD have an average DIN : DIP ratio of 70, which was able to seriously affect the ecological environment. The SGD-derived nutrient fluxes were higher than the local river input, which demonstrated that the SGD was a major source of nutrients affecting regional marine ecosystems.

KEYWORDS

Radium isotopes, Liaodong Bay, Apparent water age, SGD-derived nutrient, SGD

1 Introduction

Submarine groundwater discharge (SGD) is regarded as any seaward flux of water from the rock pores and fractures on continental margins to the coastal ocean, without considering the constituents of flow or driving forces (Burnett et al., 2003). The SGD consists of freshwater from inland and recirculated seawater discharge through

sediments, both of which are important pathways for delivering biochemical substances from land to sea, such as nutrients (Zhang et al., 2016; Liu et al., 2017; Prakash et al., 2020), heavy metals (Ganguli et al., 2012; Wang et al., 2019), and organic contaminants (Taniguchi et al., 2019). A series of reactions of biology and chemistry may occur in the saltwater and freshwater interaction zone due to the migration of a large number of nutrient loadings and heavy metals (Beck et al., 2007; Zhang et al., 2020a; Santos et al., 2021). The accurate assessment of SGD and associated nutrient fluxes is very important for water resource management and ecological environment protection (Burnett et al., 2006; Li and Wang, 2015; Wang et al., 2018).

The quantitative study of SGD is challenging because of the variability in the spatial distribution of SGD. Over the past years, the common methods used for determining the SGD include direct measurement (Debnath and Mukherjee, 2016; Prakash et al., 2018), analytical solution (Guo and Li, 2015), numerical simulation (Vaeret et al., 2012; Gopinath et al., 2016; Gopinath et al., 2019), and isotope tracing method (Moore, 1996; Moore, 2007; Luo and Jiao, 2016; Liu et al., 2019; Lopez et al., 2020; Wang et al., 2020b). Among them, the isotope tracing method is the most effective method to quantify SGD at a large scale (Lopez et al., 2020; Wang et al., 2020c). Typically, Moore (1996) used ^{226}Ra to assess the SGD along the 320-km-long coastline of the eastern United States. Since then, radium isotopes have been widely used to evaluate SGD in many places of the world, including the Okatee Estuary, USA (Moore et al., 2006); Southeastern Continental Shelf, USA (Moore, 2007); Upper Atlantic Ocean, USA (Moore, 2008); Tolo Harbour, Hong Kong (Lee et al., 2012); Geoje Bay, Korea (Hwang et al., 2016); the Yellow Sea, China (Kim et al., 2005); Laizhou Bay, China (Wang et al., 2020c); Jiaozhou Bay, China (Zhang et al., 2017); and numerous other sets of the world.

Radium isotope tracing is indeed a relevant method due to the wide range of radium isotope half-lives, which are between 3.63 days for ^{224}Ra and 1,600 years for ^{226}Ra (Webster et al., 1995; Moore et al., 2006). The mass balance model comprising each key chemical substance in the aquifer and seawater is established by taking the SGD as the main pathway. The sources of radium isotopes are mainly diffusion from sediments, river input, suspended particulate matter desorption, and SGD input. The mixing loss with open seawater and radioactive decay are the sinks of radium isotopes. The radium isotopes of ^{223}Ra and ^{224}Ra are more suitable for studying the water cycle process with a short time scale in a small distribution area, compared with the radium isotopes of ^{226}Ra and ^{228}Ra. They can be used to estimate the mixing rate and diffusivity effectively (e.g., Luo et al., 2014; Luo and Jiao, 2016). For example, Liu et al. (2015) estimated the SGD in the embayment of Bohai Sea, China, using the short-lived isotopes ^{223}Ra and ^{224}Ra. Xiao et al. (2019) assessed the groundwater discharge rate based on the model of radium mass balance using ^{223}Ra and ^{224}Ra in a typical urbanized estuary in China.

Previous studies have revealed that the SGD is an important nutrient loading source, which is transported from groundwater to seawater (e.g., Makings et al., 2014; Zhang et al., 2016; Wang et al., 2020b). Recently, Cho et al. (2018) found that dissolved inorganic nitrogen (DIN) and dissolved inorganic phosphorus (DIP) from SGD were 0.7~1.4 times higher than those from the river input on a global scale. On a local scale, the ratio of nutrient flux carried by the SGD to that from the river input may be higher. For example, the SGD-associated nutrient loadings in the Yellow River Estuary were at least five times greater than those from the river input (Xu et al., 2013). As a result, eutrophication occurred and nutrient structures (e.g., N/P ratio) were changed by the accumulation of nutrients in the ocean. For instance, the prominent problem was eutrophication caused by the discharge of nutrients, and the growth of phytoplankton was restricted by phosphorus (P) in Bohai Bay, China (Peng, 2015; Qiao et al., 2017). Therefore, to better protect the marine ecological environment, it is of great importance to assess the SGD-derived nutrient fluxes.

Although the SGD has been estimated in many coastal aquifers of China based on the method of isotope tracing (e.g., Wang et al., 2015; Zhang et al., 2017; Xiao et al., 2019; Wang et al., 2020b), there is no study on the SGD and its nutrient inputs in the eastern coastal zone of Liaodong Bay, China. Liaodong Bay is situated in the northeast of Bohai Sea. It is one major water body of the Bohai Sea. It is a typical semi-enclosed embayment. In recent years, with the rapid economic growth in Liaodong Bay, the impacts of human activities on the bay become more frequent (Ma and Wang, 2003; Guo et al., 2020a). Liaodong Bay has become one of the most polluted marine areas in China (Song and Duan, 2019; Wang et al., 2020). A large number of eutrophic substances are discharged into the sea from the rivers in coastal zones, which leads to serious eutrophication problems in Liaodong Bay (Wang et al., 2009; Cai et al., 2013; Pei et al., 2019). However, it is not known how much nutrients are brought into the sea through the SGD in eastern Liaodong Bay. Thus, it is important to carry out the research on SGD and its associated nutrients for the assessment of the ecological environment in eastern Liaodong Bay.

This study aims to estimate the SGD and its associated nutrients in eastern Liaodong Bay, China. The spatial distributions of the short-lived radium isotopes ^{223}Ra and ^{224}Ra were studied. The impacts of the geochemical environmental factors and human activities on the activities of ^{223}Ra and ^{224}Ra were then analyzed and discussed. The radium isotopes ^{223}Ra and ^{224}Ra were used to determine the SGD based on the mass balance model. The pollution of water due to dissolved inorganic nitrogen and phosphorus (DIN and DIP) was discussed, and the nutrient fluxes derived from the SGD were estimated.

2 Study area

Liaodong Bay (located between 117°35′ and 122°15′E longitude and 37°07′ and 41°N latitude) is part of the Bohai Sea and situated in the northern part of the Bohai Sea in northeastern China. It is a nearly closed interior sea (Guo et al., 2020b). Its waters span ~10,000 km^2 and its mean water depth is 22 m. The research area is situated in the coastal zone, in the eastern part of Liaodong Bay, as described in Figure 1. Geographically, the area is situated at 121°37′ to 122°24′E longitude and 40°3′ to 40°39′N latitude. It starts from the Daliao River in the north to the Fudu River in the south of the coastal area in Yingkou City, Liaoning Province. The total length of the coastline is about 76 km.

The research area has a semihumid climate (temperate zone): It is hot and rainy in summer but cold and dry in winter. The annual average temperature of the study area is 9.4°C. The highest temperature (37°C) occurs in July and the lowest temperature (−21°C) occurs in January.[1] The annual precipitation ranges from 600 to 800 mm, and the evaporation for each year is between 1,000 and 1,200 mm (Zhu et al., 2020). The main rainfall intensities occur from July to September, which is about 80% of the annual precipitation (Pei et al., 2019). The coastal zone of the research area is mainly affected by tide, wave, and current. Most of the tides are reciprocating tides and regular semidiurnal tides (Li et al., 2021).

The landform of the eastern coast of Liaodong Bay area changes from the eastern part to the western part regularly, due to the effects of structure, lithology, and neotectonic movement TSGSBOLP (The Seventh Geological Survey Brigade of Liaoning Province), 1973. Generally speaking, the geomorphic types are low mountains, high and low hills, and alluvial plains from east to west (Zhu et al., 2020). The alluvial plain in the research area is bordered by the mountains in the eastern part and by the sea in the western part (Figure 1). The terrain of the alluvial plain slows down from east to west gradually. In the coastal zone, the beach is mainly composed of silty and fine sand, which is distributed in the shallow area. The sandy sediments are mainly distributed in the nearshore areas (Xiong et al., 2020). There is a small amount of sandy silt and silty sand in the seabed. From north to south, the main rivers in Yingkou City are the Daliao River, Daqing River, Shahe River, Xiongyue River, and Fudu River, which flow into the sea from the eastern part to the western part. Among them, the Daliao River is the biggest, and its discharge is almost the same as that of the Yellow River (Ye et al., 2015). According to the data provided by the local hydrological bureau, the total runoff of the rivers is about 3.98×10^6 m^3 day^{-1}.

The groundwater flows in the quaternary loose sediments of the Liaodong littoral plain area. The aquifer type is mainly alluvium of Holocene and upper Pleistocene (TSGSBOLP). The aquifer in the research area is mainly recharged vertically. The sources consist of precipitation, lateral replenishment from the river, irrigation recharge, and runoff at the mountain front. The form of groundwater discharge includes the discharge to the river, groundwater runoff, evaporation, and artificial exploitation. The groundwater flows from east to west, and its velocity changes with the aquifer thickness, permeability, and topography (Zhu et al., 2020). The velocity of groundwater flow decreases in the coastal zone as the hydraulic conductivity of the aquifer decreases. Moreover, the amount of groundwater exploitation is larger than that of recharge, due to the rising demand for water in the Yingkou area, under the influences of urban development and human activities. The groundwater level in the aquifer decreases because of the imbalance of pumping and recharge. As a result, the seawater intrusion area is mainly distributed in the sandy aquifer of the coastal zone. The phenomenon of seawater intrusion was investigated in the silt coastal zone, such as the Daqing River estuary (Ma et al., 2019; Zhu et al., 2020).

Nutrient pollution and eutrophication have become increasingly serious in the estuaries of eastern Liaodong Bay due to the discharged wastewater from human activities and industries and due to agricultural fertilizer pollution (Pei et al., 2019). Nutrient pollution was carried into the sea through river input and SGD. However, the rivers were cut off and dried up usually in the year because the rivers were developed and utilized in the upstream areas. Thus, a large quantity of nutrients is brought into the sea through the SGD in eastern Liaodong Bay. In addition, heavy metal pollution in eastern Liaodong Bay is also serious, and heavy metal contaminants, such as Cd, Hg, and As, are most prominent in this area (Lan et al., 2018; Wang et al., 2020).

3 Materials and methods

3.1 Field survey and sampling

The field campaign was carried out from 23 to 25 September 2019 in eastern Liaodong Bay. As shown in Figure 1, the coast of the Daliao River was taken as the boundary because the daily average runoff of the Daliao River was higher than the sum of the daily runoff of other rivers, and the economy was developed and the population activities were concentrated in the Daliao River Basin. There were 41 sampling sites in the area (Figure 1). The features of the selected sample sites are listed in Table 1. There were 41 samples collected in the study area: 9 samples of groundwater, 25 samples of seawater, and 7 samples of river water. The groundwater samples (from GW1 to GW9) were set along the coastline. They were obtained at depths between 0.3 and 1.0 m, with a volume of 5–10 L. The water was pumped out using a peristaltic pump after inserting the push point piezometer into the deposited sediment. At each position, the samples of seawater (from SW1 to SW25) were sampled from depths ranging from 1 to 2 m below the seawater surface, with a volume of 60 L for each sample. One or two samples were collected from each river, and the volume of each sample was 30 L.

1 http://data.cma.cn/

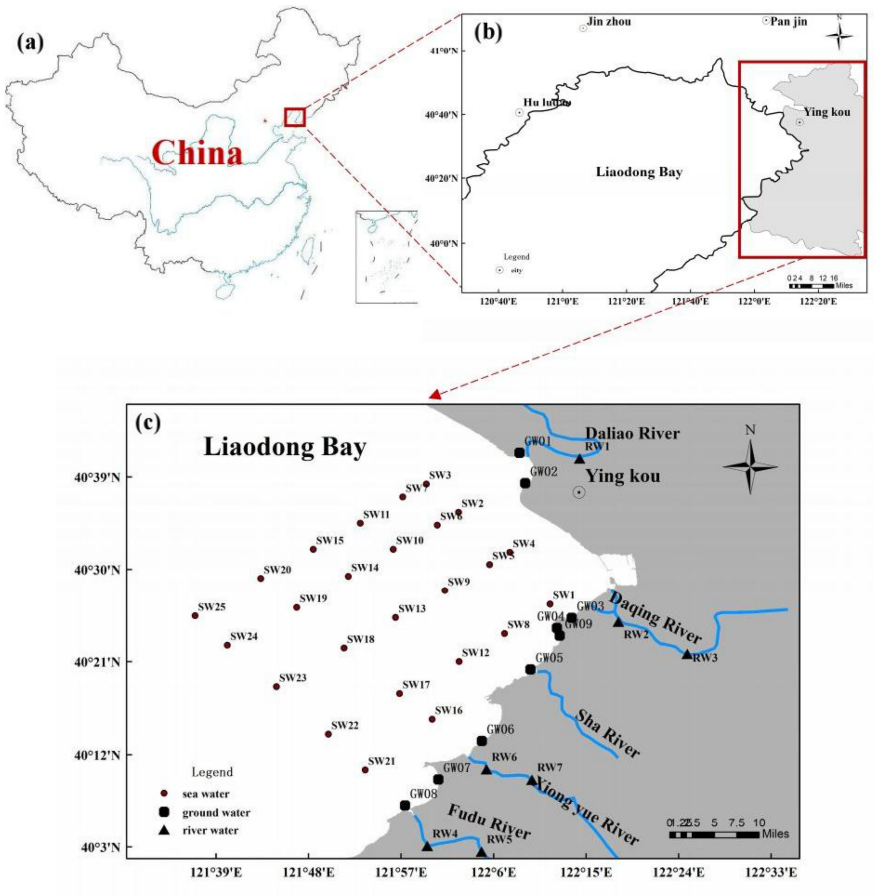

FIGURE 1
(A–C) The distribution of sampling points in the Yingkou area of Liaodong Bay in the study area. The rhombi, triangles, and circles represent the sampling points of river water, groundwater, and seawater, respectively.

The radium isotopes in all the water samples were enriched with Mn fibers, which were made by acrylonitrile fibers (white and heat resistant, 100% acrylic fiber material) (Moore and Reid, 1973). They were boiled until their color became dark brown with 0.5 mol/L of potassium permanganate solution at the temperature of 70–80°C. During the process of preparation, the original toughness of acrylonitrile fibers cannot be reduced. After the preparation, in order to remove the manganese oxide on the surface of Mn fibers, they were quickly rinsed with pure water until the color of the water remained unchanged. Then, after drying, they were put into a sealed bag for the experiment.

During sampling, the radium was withdrawn when the water flowed through a cartridge. The Mn fibers of about 25 g were filled into the cartridge. In order to extract the radium isotopes quantitatively, the water flow velocity of the sample had to be smaller than 1 L/min by controlling the tap at the bottom of the sampling bucket (Moore and Reid, 1973). After the enrichment, the Mn fibers were taken out. In order to remove all salts and particles on the Mn fibers, they were flushed with distilled water. They were later measured for radium isotope activity within 24 h in the laboratory.

The samples for detecting nutrients were filtered using a 0.45-μm filter, which were collected in plastic vials (40 ml). The nutrient samples were immediately frozen after filtering to analyze the DIN and DIP. The water samples were sampled in 1 L bottles, which were labeled for analyzing the major ions. The impurities in the water were filtered using a 0.45-μm polypropylene filter element. A portable HI9828 model probe (Hanna, Italy) was used to measure the salinity, temperature, and electrical conductivity (EC) of the samples at the field site (Wang et al., 2016). The information about the sampling positions, amount of sample, and time was recorded during the sampling.

3.2 Laboratory measurement

The ^{223}Ra and ^{224}Ra activities in surface water and groundwater were detected using the Radium Delayed

TABLE 1 The activity concentrations of ^{223}Ra and ^{224}Ra as well as salinity at each sample point in the research area.

Sample	Longitude	Latitude	Salinity (psu)	^{223}Ra activity (dpm 100 L^{-1})	^{224}Ra activity (dpm 100 L^{-1})	^{224}Ra/^{223}Ra AR
SW1	122.19	40.44	27.06	1.73 ± 0.21	65.54 ± 4.59	37.88 ± 3.41
SW2	122.04	40.59	31.25	1.65 ± 0.20	56.03 ± 3.92	33.96 ± 3.12
SW3	121.99	40.64	36.2	–	54.3 ± 3.8	–
SW4	122.13	40.53	27.12	1.06 ± 0.13	68.71 ± 4.81	64.82 ± 5.34
SW5	122.09	40.51	30.05	2.27 ± 0.27	53.62 ± 3.75	23.62 ± 2.35
SW6	122.01	40.57	34.2	1.66 ± 0.20	28.49 ± 1.99	17.16 ± 1.87
SW7	121.95	40.62	27.62	1.19 ± 0.14	65.49 ± 4.58	55.03 ± 4.61
SW8	122.12	40.40	35.21	1.58 ± 0.19	72.49 ± 5.07	45.88 ± 3.98
SW9	122.02	40.47	29.65	1.82 ± 0.22	94.76 ± 6.63	52.07 ± 4.42
SW10	121.94	40.53	28	2.75 ± 0.33	55.75 ± 3.9	20.27 ± 2.11
SW11	121.88	40.57	27.21	2.93 ± 0.35	87.94 ± 6.16	30.01 ± 2.83
SW12	122.04	40.35	30.2	3.24 ± 0.39	51.48 ± 3.6	15.89 ± 1.77
SW13	121.94	40.42	36.2	1.31 ± 0.16	41.83 ± 2.93	31.93 ± 2.98
SW14	121.86	40.49	30.25	1.94 ± 0.23	42.43 ± 2.97	21.87 ± 2.22
SW15	121.81	40.53	26.22	2.45 ± 0.29	71.75 ± 5.02	29.29 ± 2.77
SW16	122.00	40.26	33.53	2.08 ± 0.25	38.59 ± 2.7	18.55 ± 1.98
SW17	121.95	40.30	33.28	–	20.02 ± 1.41	–
SW18	121.78	40.44	33.17	1.21 ± 0.15	13.41 ± 0.94	11.08 ± 1.41
SW19	121.86	40.37	34.65	–	19.55 ± 1.37	–
SW20	121.72	40.49	31.86	2.52 ± 0.3	48.06 ± 3.36	19.07 ± 2.01
SW21	121.89	40.18	35.13	0.72 ± 0.09	15.61 ± 1.09	21.68 ± 2.24
SW22	121.83	40.23	36.2	1.33 ± 0.16	20.89 ± 1.46	15.71 ± 1.76
SW23	121.75	40.31	33	1.44 ± 0.17	10.55 ± 0.74	7.33 ± 1.06
SW24	121.67	40.38	21	1.47 ± 0.26	45.31 ± 3.17	30.82.42 ± 3.18
SW25	121.62	40.42	34.7	1.54 ± 0.18	40.35 ± 2.82	26.2 ± 2.53
GW1	122.14	40.69	15	2.92 ± 0.11	113.69 ± 7.96	38.93 ± 2.98
GW2	122.15	40.64	15	4.84 ± 0.58	240.73 ± 16.85	49.74 ± 4.25
GW3	122.23	40.42	30	31.91 ± 0.8	737.73 ± 51.64	23.12 ± 1.79
GW4	122.20	40.40	29	25.79 ± 0.1	1,244.87 ± 87.14	48.27 ± 3.41
GW5	122.16	40.34	12	12.24 ± 0.47	1,103.5 ± 77.25	90.16 ± 6.58
GW6	122.08	40.22	29.5	58.88 ± 0.07	2,103.78 ± 147.26	35.73 ± 2.51
GW7	122.01	40.16	35	27.6 ± 0.31	1,729.51 ± 121.07	62.66 ± 4.47
GW8	121.96	40.12	30.4	4.83 ± 0.58	641.82 ± 44.93	132.88 ± 10.12
GW9	122.21	40.39	10	4.62 ± 0.07	271.84 ± 19.03	58.84 ± 4.23
RW1	122.24	40.68	7	0.85 ± 0.1	76.8 ± 5.38	90.35 ± 7.12
RW2	122.30	40.41	0	1.24 ± 0.15	17.23 ± 1.21	13.9 ± 1.62
RW3	122.41	40.36	0	1.34 ± 0.16	22.87 ± 1.60	17.07 ± 1.86
RW4	121.99	40.05	0.4	0.27 ± 0.03	41.38 ± 2.90	153.26 ± 11.5
RW5	122.07	40.04	0.3	0.43 ± 0.05	32.11 ± 2.25	74.67 ± 6
RW6	122.09	40.09	0.28	1.06 ± 0.11	43.31 ± 3.03	40.86 ± 3.52
RW7	122.04	40.10	0.32	0.94 ± 0.13	29.98 ± 2.10	31.89 ± 3.07

– denotes the data being abnormal.

Coincidence Counter (RaDeCC) instrument (produced by the Scientific Computer Instruments Company, USA). It was widely used in radium isotope measurement. The measurement method was presented in Moore and Krest (2004) and Moore (2008). The half-life of the short-lived isotope ^{224}Ra was 3.66 days; therefore, the measurement was completed in 3 days. In order to prevent the influence of ^{223}Ra decay, the measurement of short-lived isotope ^{223}Ra was carried out within 7–9 days after sampling. After the two measurements, the samples were stored for about 30 days, and then the isotope ^{228}Th was

measured to correct ^{224}Ra produced by ^{228}Th. The initial ^{224}Ra activity was thus obtained. The measurement uncertainty of ^{223}Ra and ^{224}Ra was about 12% and 7%, respectively.

After taking the water samples to the laboratory for nutrient measurement, they were immediately filtered with a 1-μm polypropylene filter cartridge, and the impurities were filtered with a 0.45-μm filter membrane. Then, flow injection analysis (FIA) utilizing an autosampler and spectrophotometric measurements were conducted to analyze the DIN (NO_3^-, NO_2^-, and NH_4^+) and DIP. The uncertainty of measurement was 3%, 8%, 10%, and 5% for NO_3^-, NO_2^-, NH_4^+, and DIP, respectively. The method of Wang et al. (2002) was used to measure DIN (the sum of NH_4^+, NO_2^-, and NO_3^-) and DIP.

Cations and anions were analyzed at the Jiangsu Geological Survey Institute, China. The samples were analyzed for HCO_3^-, Cl^-, SO_4^{2-}, NO_3^-, Na^+, K^+, Ca^{2+}, and Mg^{2+} after filtering. The HCO_3^- ion concentrations were obtained based on the measured pH and total alkalinity (TA). The anions (Cl^-, SO_4^{2-}, and NO_3^-) were determined based on the ion chromatography (DX-120, Dionex, America). The cations (Na^+, K^+, Ca^{2+}, and Mg^{2+}) were detected by ICP-AES (Thermo ICAP6300, America). The lower limit of detection was set to 0.01 mg L^{-1} for these ions.

3.3 Radium ages

The apparent water age can reflect the renewal and purification capacity of a water body, which is very important to study the hydrodynamic process of water and its components transported to the sea (Moore, 2000). The apparent water age is a comprehensive parameter describing the characteristics of water body exchange, ignoring the physical processes under surface water and the spatial distribution of these processes. Moore (2000) proposed a method to estimate the apparent water age by using the ^{224}Ra/^{223}Ra activity ratio (AR). The initial value of ^{224}Ra/^{223}Ra AR was a constant value (Moore et al., 2006). The ratio varied with the radioactive transformation; thus, the apparent water age could be estimated by the following equation (Moore, 2000):

$$\left[\frac{^{224}Ra}{^{223}Ra}\right]_i = \left[\frac{^{224}Ra}{^{223}Ra}\right]_{GW} \frac{e^{-\lambda_{224}T_f}}{e^{-\lambda_{223}T_f}} \quad (1)$$

Equation (1) can be further transformed into (Moore, 2000)

$$T_f = \frac{\ln\left(\frac{^{224}Ra}{^{223}Ra}\right)_i - \ln\left(\frac{^{224}Ra}{^{223}Ra}\right)_{GW}}{\lambda_{223} - \lambda_{224}}, \quad (2)$$

where $\left(\frac{^{224}Ra}{^{223}Ra}\right)_i$ is the ^{224}Ra/^{223}Ra activity ratio of the observed point i in seawater; $\left(\frac{^{224}Ra}{^{223}Ra}\right)_{GW}$ denotes the ^{224}Ra/^{223}Ra activity ratio of groundwater entering into the study area; λ_{223} is the ^{223}Ra decay constant and its value is 0.0608 $days^{-1}$; λ_{224} is the ^{224}Ra decay constant and its value is 0.189 $days^{-1}$; and T_f is the apparent water age.

3.4 SGD estimates

The radium isotopes in seawater were mainly from the SGD input, river input, sediment diffusion and desorption, and desorption of suspended particulate matters from rivers; the output items mainly included the mixture loss with offshore water and radioactive decay (Dulaiova and Burnett, 2008). The input fluxes from the dust deposit and precipitation were not considered because they were insignificant and negligible (Zhang et al., 2017). Through analyzing the source and sink terms in the study area and using the short-lived isotope ^{224}Ra, the mass balance equation of radium was built to calculate the SGD. The formula can be expressed as follows (Charette et al., 2003; Lamontagne et al., 2015):

$$F_{SGD} + F_{river} + F_{sed} + F_{sp} = F_{decay} + F_{mixing} \quad (3)$$

where F_{SGD} is the ^{224}Ra flux from the SGD input, F_{river} is the ^{224}Ra flux from the river input, F_{sed} is the ^{224}Ra flux of diffusion of sediments, F_{sp} represents the ^{224}Ra flux of suspended particulate matter desorption in the river, F_{decay} is the ^{224}Ra flux from radioactive decay, and F_{mixing} represents the amount of ^{224}Ra flux mixing with the outer seawater.

During the sampling process, there was no rainfall in the study area. The time for sampling was during the terminal rainy season. Therefore, the input of radium caused by precipitation was ignored. The river was clear and free of impurities; therefore, the radium ^{224}Ra flux from riverine particulate desorption F_{sp} in Eq. (3) was neglected.

The equation for calculating the amount of ^{224}Ra in the river in Eq. (3) is as follows (Li et al., 2019):

$$F_{river} = \sum_{i=1}^{n} Q_{r,i}\, ^{224}Ra_{RW,i} \quad (4)$$

Where $Q_{r,i}$ denotes the flux of the river (m^3/day) the i-th river (dpm 100 L^{-1}).

The diffusion from the sediment of the seafloor is one of the sources of ^{224}Ra activity. The ^{224}Ra isotope is desorbed from the seafloor and transported to the upper ocean through physical mixing, bioturbation, and biological irrigation (Moore, 2007). The diffusion flux ^{224}Ra of surface sediment is calculated as follows (Moore, 2007; Tang et al., 2015):

$$F_{sed} = A_{sed} \times D_{sed}, \quad (5)$$

where A_{sed} denotes the area of seafloor sediments, which is the area of the sea in the research area (m^2), and D_{sed} indicates the diffusion flux per unit sediment area (dpm m^{-2} day^{-1}).

The mixing loss of ^{224}Ra includes the mixing diffusion of radioactive decay. The formula of the mixed diffusion term is as follows (Kim and Kim, 2011; Luo et al., 2014):

$$F_{mixing} = \frac{V_{bay}\left(^{224}Ra_{bay} - ^{224}Ra_{sea}\right)}{T_f} \quad (6)$$

where V_{bay} represents the volume of seawater, $^{224}Ra_{bay}$ is the average activity of ^{224}Ra in the sea of the study area (dpm 100 L^{-1}), and $^{224}Ra_{sea}$ is the activity of ^{224}Ra contributed by the open sea (dpm 100 L^{-1}).

In addition, the calculation formula of ^{224}Ra radioactive decay is as follows (Zhang et al., 2017; Wang et al., 2020c):

$$F_{decay} = \lambda_{224} V_{bay}\, {}^{224}Ra_{bay}\,. \quad (7)$$

The F_{SGD}can be obtained by substituting F_{river}, F_{sed}, F_{mixing}, and F_{decay} into Eq. (3). Then, the volume flow $V_{SGD}$of SGD in the study area can be obtained, combined with the activity of groundwater (Zhang et al., 2017; Wang et al., 2020c),

$$V_{SGD} = \frac{F_{SGD}}{{}^{224}Ra_{GW}} \quad (8)$$

where $^{224}Ra_{GW}$ is the ^{224}Ra activity in the groundwater end-member (dpm 100 L^{-1}).

4 Results

4.1 Distribution of salinity and radium isotopes

The temperature of seawater varied between 14.4°C and 22.1°C, with an average value of 20.51°C, and that of coastal groundwater was between 18.8°C and 25.0°C, with an average value of 20.83°C. The temperature within the river water varied between 20.9°C and 22.5°C, with an average value of 21.53°C. The activity of ^{223}Ra and ^{224}Ra in seawater, river water, and groundwater, as well as salinity, is reported in Table 1.

From Figure 2A, one can see that salinity in surface seawater varied slightly, ranging from 26.22 to 36.2, with an average value of 31.76. The salinity of groundwater ranged from 10 to 35, with an average value of 22.88 (Table 1). The salinity in river water was between 0 and 7.0, and its average value was 1.19 (Table 1). From Figures 2B, C, one can see that the activities of ^{223}Ra and ^{224}Ra in seawater were between 0.72 and 3.24 dpm 100L^{-1} and between 10.55 and 94.76 dpm 100L^{-1}, with average values of 1.81 and 47.32 dpm 100 L^{-1}, respectively. The ^{223}Ra and ^{224}Ra activities in river water ranged from 0.27 to 1.34 dpm 100 L^{-1} and from 17.23 to 76.8 dpm 100L^{-1}, with average values of 0.87 and 37.67 dpm 100 L^{-1}, respectively. In coastal groundwater, the activities of ^{223}Ra and ^{224}Ra ranged from 2.92 to 58.88 dpm 100L^{-1} and from 113.69 to 2,103.78 dpm 100L^{-1}, with average values of 19.29 and 909.72 dpm 100L^{-1}, respectively. The average value of the activity of ^{223}Ra in coastal groundwater was 61.45 times higher than that in seawater and 130.68 times higher than that in river water, respectively. The average ^{224}Ra activity in coastal groundwater was 19.22 times higher than that in seawater and 24.15 times higher than that in river water, respectively. The activities of radium isotope in coastal groundwater were higher because they were desorbed from the particles in the freshwater and saltwater interaction zone. The activities of radium isotopes in surface seawater were lower than those in coastal groundwater, which indicated that the radium isotopes in the bay area were mainly from the SGD (Tang et al., 2015; Wang et al., 2020b).

Figure 3A shows that salinity in seawater increased with the offshore distance from the coast of the Daliao River to the sea. From Figures 3B, C, it can be seen that ^{223}Ra and ^{224}Ra activities were reasonably elevated in the nearshore areas. Then, the activities of ^{223}Ra and ^{224}Ra were reduced with the increase of offshore distances generally. The reason was that the decrease in radium activities mainly resulted from the lack of support from the parent decay in the sediments or particles. Figure 4 shows that ^{223}Ra activity was positively correlated to ^{224}Ra activity in seawater. The activity of ^{224}Ra increased with the activity of ^{223}Ra, which indicated that ^{223}Ra and ^{224}Ra activities in seawater had the same sources. In addition, the value of ^{224}Ra/^{223}Ra RA became smaller as groundwater was discharged into seawater because the decay rate of ^{224}Ra was faster than that of ^{223}Ra in coastal seawater.

4.2 Major elements

The measured values of total dissolved solids (TDS), electrical conductivity, and concentrations of major ions for the samples of seawater, river water, and groundwater are summarized in Table 2. During the mixed process of river water, groundwater, and seawater, the conditions of the water body change and the adsorption–desorption and precipitation–dissolution between the dissolved liquid phase and solid phase of the chemical substances may occur in the water body. As a result, the concentrations of chemical components in different water bodies change. The average concentrations of the main cations in seawater were 348.0, 947.33, 492.0, and 8,801.0 mg L^{-1} for Ca^{2+}, Mg^{2+}, K^{+}, and Na^{+}, respectively. The order of abundance of the cations was Na^{+} > Mg^{2+} > K^{+} > Ca^{2+} in seawater. Generally speaking, the cation concentrations (K^{+}, Ca^{2+}, Na^{+}, Mg^{2+}) in seawater increased as the salinity increased in the mixed process of freshwater and saltwater. The order of the abundance of cation concentrations in different water bodies was seawater > groundwater > river water. The average concentrations of Cl^{-}, NO_3^{-}, SO_4^{2-}, and HCO_3^{-} in seawater were 16,266.33, 6.87, 2,371.17, and 160.17 mg L^{-1}, respectively. The orders of the abundance of anion concentrations in different water bodies were as follows: seawater > groundwater > river water for SO_4^{2-}, river water > groundwater > seawater for NO_3^{-}, groundwater > seawater > river water for Cl^{-}, and groundwater > river water > seawater for HCO_3^{-}.

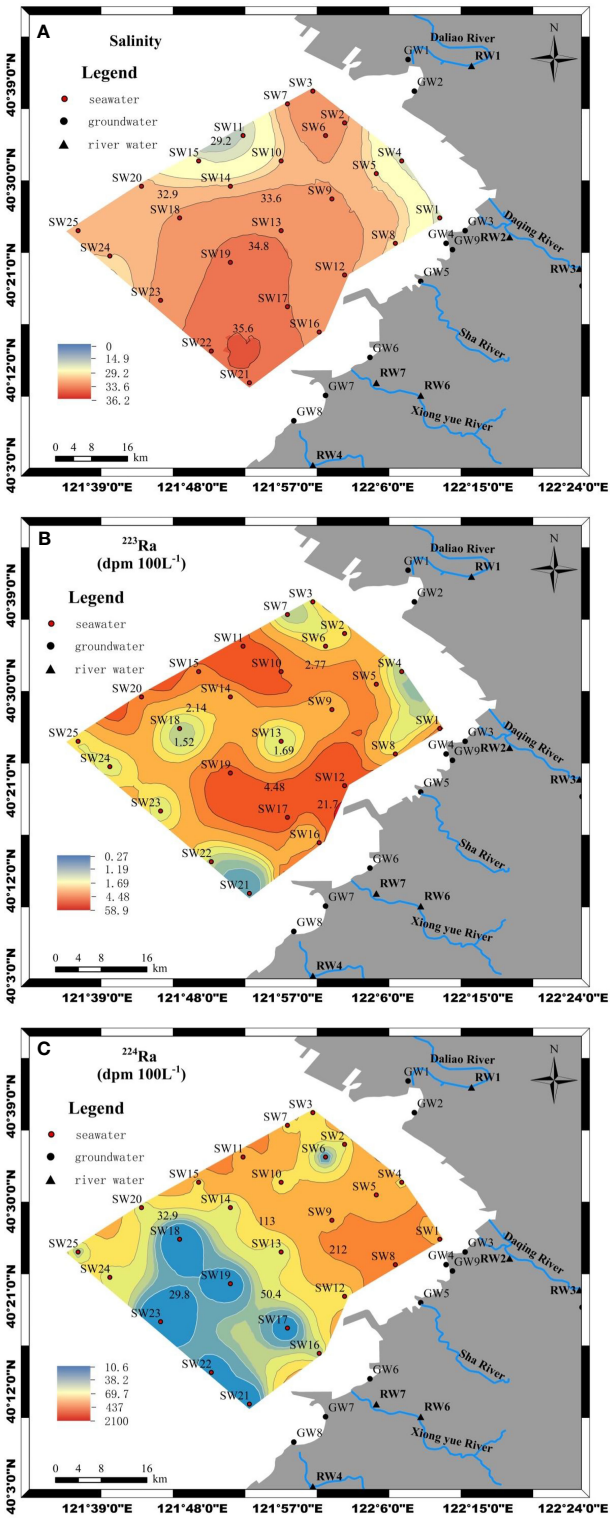

FIGURE 2
Spatial distribution map of salinity **(A)**, ^{223}Ra **(B)**, and ^{224}Ra **(C)** in the sea area of Yingkou City, Liaodong Bay.

10.3389/fmars.2022.916109

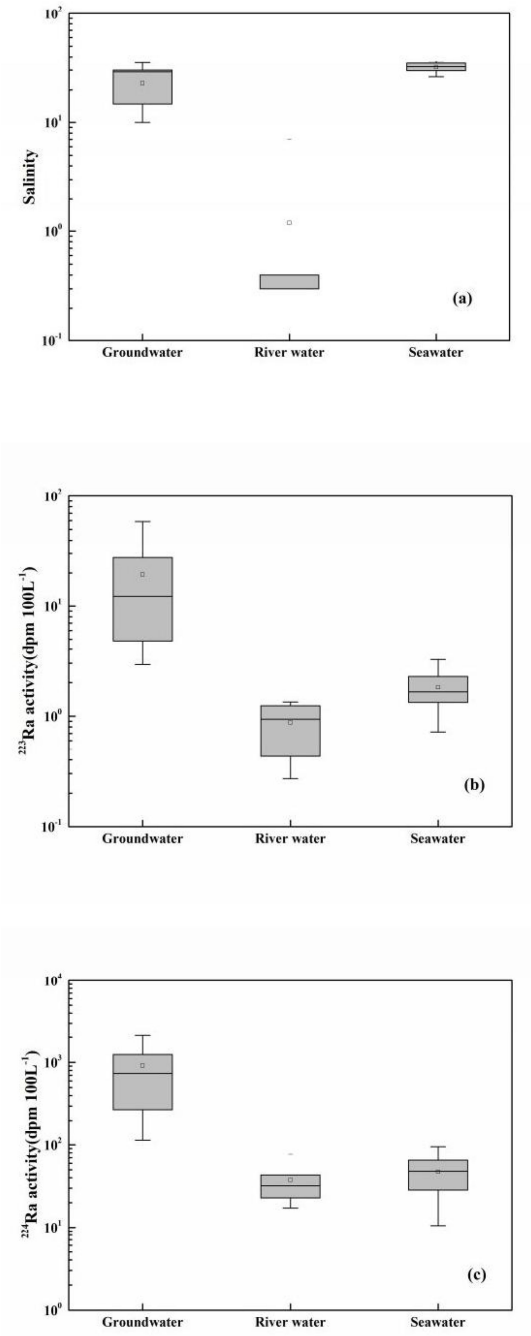

FIGURE 3
The box plot for salinity **(A)**, ^{223}Ra **(B)**, and ^{224}Ra **(C)** in groundwater, river water, and seawater.

4.3 Nutrient

The nutrient concentrations of DIP and DIN (including NO_3^-, NO_2^-, and NH_4^+) in the samples of groundwater, seawater, and river water are summarized in Table 3. The average values of nutrient concentrations were 7.75 μmol L^{-1} for DIP, 546.66 μmol L^{-1} for DIN, 412.79 μmol L^{-1} for NO_3^-, 7.03 μmol L^{-1} for NO_2^-, and 123.1 μmol L^{-1} for NH_4^+ in the samples of groundwater. The average nutrient concentrations in the river water samples were 9.8μmol L^{-1} for DIP, 865.97 μmol L^{-1} for DIN, 756.47μmol L^{-1} for NO_3^-, 9.02μmol L^{-1} for NO_2^-, and 94.83μmol L^{-1} for NH_4^+. The average nutrient concentrations in

10.3389/fmars.2022.916109

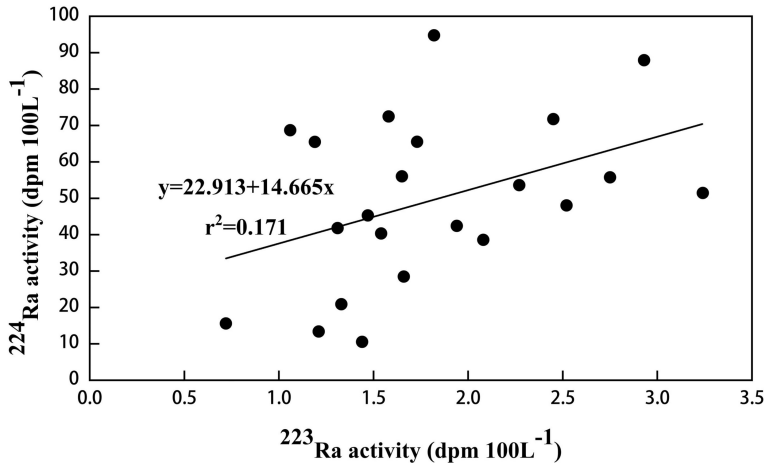

FIGURE 4
The correlation between the activities of ^{223}Ra and ^{224}Ra.

the seawater samples were 4.69μmol L^{-1} for DIP, 163.79μmol L^{-1} for DIN, 110.81μmol L^{-1} for NO_3^-, 3.81μmol L^{-1} for NO_2^-, and 46.91μmol L^{-1} for NH_4^+. Therefore, the order of the abundance of DIN, DIP, NO_3^-, and NO_2^- was river water > groundwater > seawater, whereas the NH_4^+ in the water body followed the order of groundwater > river water > seawater.

TABLE 2 The measured data of physics and chemistry obtained for the samples of seawater, groundwater, and river water.

Sample	Electrical conductivity (IS cm^{-1})	TDS (g L^{-1})	Ca^{2+} (mg L^{-1})	Mg^{2+} (mg L^{-1})	Na^+ (mg L^{-1})	K^+ (mg L^{-1})	NO_3^- (mg L^{-1})	SO_4^{2-} (mg L^{-1})	Cl^- (mg L^{-1})	HCO_3^- (mg L^{-1})
SW3	46.78	30.25	349	1,042	8,718	444	6.84	2,320	16,416	161
SW8	42.93	29.49	348	996	8,727	480	8.24	2,274	15,608	155
SW13	48.04	31.63	338	879	8,596	482	4.76	2,255	16,057	155
SW18	48.92	33.79	345	917	8,643	495	5.87	2,314	16,147	168
SW22	49.5	36.82	377	967	9,612	554	8.9	2,523	17,672	161
SW24	34.76	17.6	338	883	8,510	497	6.61	2,541	15,698	161
GW01	21.66	14.9	218	468	4,339	180	20.2	1,120	8,073	226
GW02	18.73	13.05	171	379	3,817	179	18.7	980	6,638	232
GW03	7.1	5.71	50.9	25.2	116	12.3	5.93	33.5	154	336
GW04	45.33	29.97	343	867	8,588	453	27.2	2,226	15,788	174
GW05	39.76	27.34	322	835	8,074	456	15.4	2,147	14,891	181
GW06	16.44	12.17	164	45.3	173	12.3	61.2	331	269	232
GW08	43.51	32.59	376	1,020	9,565	534	23.4	2,504	17,223	168
GW09	46.7	33.43	388	1,048	10,220	593	9.86	2,610	18,030	148
GW10	45.01	33.31	367	984	9,673	568	6.44	2,466	17,851	148
GW11	18.76	12.61	115	52.1	333	27.4	67.6	224	416	439
RW01	7.5	5.23	111	156	1,417	126	3.91	416	2,601	200
RW02	4.74	2.76	44.4	16.6	28.7	13.4	35.1	75.5	43.1	136
RW03	5.28	3.67	51.6	23.2	27.8	11.4	54.4	93.2	50.2	148
RW04	6.81	4.76	60.1	17.5	41.9	10.6	60.2	98.8	43.1	129
RW05	5.82	3.01	66	16.2	30.1	10	57.5	101	39.5	123
RW06	5.7	4.23	46.4	11.2	21.2	10.3	59.8	69.1	28.7	71
RW07	5.21	3.65	42.4	10	17.8	9.8	57.4	63.6	25.1	71

TABLE 3 Nutrient concentrations in the samples of surface water and groundwater in the study area (μmol L^{-1}).

Nutrient	Groundwater		River water		Seawater	
	Range	Average	Range	Average	Range	Average
DIP	2.76–22.31	7.75	4.58–23.93	9.8	3.5–5.92	4.69
DIN	133.29–1,252.55	546.66	96.35–1,107.31	865.97	117.21–215.79	163.79
NO_3^-	95.69–987.10	412.79	63.06–970.97	756.47	76.77–143.545	110.81
NO_2^-	2.72–13.52	7.03	6.98–12.93	9.02	2.19–4.65	3.81
NH_4^+	32.95–284.67	123.1	28.53–124.22	94.83	37.76–62.66	46.91

The water body was polluted. The N/P ratio in the rivers of the study area was 88.36, which was larger than the N/P ratio of 18.0 in the river (Slomp and Van Cappellen, 2004). The N/P ratio in groundwater was 70.54, which was much higher than that in seawater (N/P ratio of 34.92). The N/P ratio of 34.92 in seawater was larger than the Redfield ratio of 16:1 (Refiled et al., 1963), which was required for phytoplankton growth in seawater (Lignell et al., 2008). It indicated that the excessive ratio of nitrogen and phosphorus in seawater was caused by the discharge from the river and groundwater, which have great impacts on the composition of nitrogen and phosphorus in the area. As a result, the degree of eutrophication in seawater was aggravated, and the water environment in the research area deteriorated. The high concentrations of N and P in the river water may be caused by the discharge of domestic and industrial wastewater, and a large quantity of nitrogen and phosphorus nutrients were imported into the river caused by the local agriculture in Yingkou City. River-derived nutrients were considered to be the most serious sources of contamination in Liaodong Bay (Pei et al., 2019). In addition, the nutrients were transported to the coast due to hydraulic gradient and groundwater flow (Taniguchi et al., 2002). However, the dilution of seawater made the content of nitrogen and phosphorus decreased. Therefore, the content of nitrogen and phosphorus in the Yingkou area can fully satisfy the condition of algae growth. Once the temperature, light, and hydrodynamic conditions meet the requirements, serious water pollution would occur.

4.4 Apparent water age and uncertainty analysis

The apparent water age of seawater was calculated using Eq. (2), which ranged from 5.6 to 22.6 days, with an average of 13.0 days, based on the value of $^{224}Ra/^{223}Ra$ AR at each sampling point (Table 1). Figure 5 shows that the apparent water age increased gradually from northeast to southwest in the seawater of the study area, and it increased as the offshore distance increased. In this model, the selection of the value of the groundwater end-member was the most important factor affecting the result (Wang et al., 2019). The maximum value of $^{224}Ra/^{223}Ra$ activity ratio in the groundwater along the coast was calculated to be 132.88. In order to verify the influence of $^{224}Ra/^{223}Ra$ activity ratio of groundwater on the model, the maximum value of $^{224}Ra/^{223}Ra$ activity ratio of groundwater (132.88) was taken to compute the apparent water age of water (Xu et al., 2013). Thus, the average age of seawater was estimated to be 13.0 days. The results showed that the selection of radium activity value of groundwater has a great impact on the average apparent water age of seawater.

5 Discussion

5.1 Factors influencing the radium isotope distribution

Previous studies have demonstrated that the main sources and abundance of radium isotopes were obviously different due to the influences of hydrogeological conditions and human activities (urbanization, marine reclamation, and aquaculture) (Tang et al., 2015). Moreover, the activities of radium isotopes from seawater were also restricted by many geochemical environmental factors, such as ionic strength, redox, and cation exchange capacity (Gonneea et al., 2008; Vinson et al., 2013; Tang et al., 2015).

5.1.1 Effect of ionic strength

The ratio of radium adsorbed on the seafloor sediment and suspended particles to that desorbed in saline water may be influenced by the ionic strength of the solution. The radium activities in the water body of the estuary and nearshore areas can be reflected by the parameters of salinity and EC indirectly because they are natural indicators for measuring the ions and TDS in the water body (Burt et al., 2013; Swarzenski et al., 2013). In groundwater of the nearshore zone, the average activities of ^{223}Ra and ^{224}Ra at the GW6, GW7, and GW8 sampling points were higher than those at the other sampling points of groundwater (Table 1). The reason was that it was related to the salinity of seawater in the coastal area. The average salinity at the GW6, GW7, and GW8 sampling points was 31.63, which was

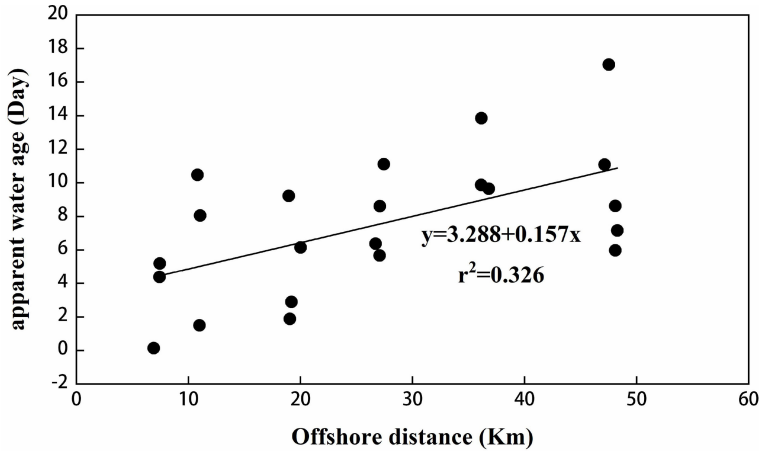

FIGURE 5
The chart of apparent water age with offshore distance.

higher than that at the other sampling points of groundwater (Table 1). It was due to the seawater invading the nearshore aquifer, which increased the salinity of groundwater. The ionic strength in the water increased, which made the radium isotopes ^{223}Ra and ^{224}Ra adsorbed on the aquifer media and the sediment surface resolved into groundwater after ion exchange (Moore, 1999). As a result, the activities of ^{223}Ra and ^{224}Ra increased.

Figure 6A shows the relationship between ^{223}Ra, ^{224}Ra, and salinity in seawater. ^{223}Ra and ^{224}Ra have a good linear correlation with salinity, that is, the activities of ^{223}Ra and ^{224}Ra decreased as the salinity increased. The main reason was that the freshwater discharged into the sea area was dominated by groundwater. The radium activity in seawater was regarded as the conservative mixing of radium activity in the coastal groundwater and river water as well as that in seawater outside the bay under ideal conditions. Thus, there was a good linear relationship between the radium isotopes ^{223}Ra and ^{224}Ra and salinity in seawater.

Figure 6B shows the variations of ^{223}Ra and ^{224}Ra activities with salinity in groundwater. One can see that the activities of ^{223}Ra and ^{224}Ra increased with salinity. The main reason was that the radium isotopes in groundwater were adsorbed by the sediment and dissolved in groundwater. The radium adsorbed on the sediment was desorbed from the sediment particles when groundwater flowed into the sea and the degree of desorption increased with salinity (Tang et al., 2015). Consequently, the activities of radium isotopes increased as the salinity increased during the process of groundwater flowing into the seawater.

5.1.2 Effect of redox

The manganese and iron oxides related to radium adsorption were sensitive to reductive dissolution, even though radium was not sensitive to redox (Gonneea et al., 2008; Vinson et al., 2013; Tang et al., 2015). Nitrate and sulfate can provide kinetic conditions for the solid-phase manganese and iron oxides removing the radium isotopes from seawater (Vinson et al., 2013). The values of SO_4^{2-} and NO_3^- in seawater increased as the offshore distance increased generally (Table 2). The increment of the concentrations of SO_4^{2-} and NO_3^- enabled the manganese and iron oxides to reduce radium activity; thus, radium activity was reduced in seawater (Vinson et al., 2013).

Figures 7A, B show the variation of the measured concentrations of SO_4^{2-} and NO_3^- in seawater with ^{223}Ra and ^{224}Ra activities. The ^{224}Ra activity decreased as the concentration of SO_4^{2-} increased; however, there was only a slight correlation between the activities of ^{223}Ra and SO_4^{2-}. The activities of ^{223}Ra and ^{224}Ra have a positive correlation with the concentrations of the NO_3^- ion. Nevertheless, the concentration of SO_4^{2-} was much higher than that of NO_3^-, and the activity of the radium isotope was mainly affected by SO_4^{2-}. Therefore, the higher concentrations of SO_4^{2-} in seawater provided support for the adsorption of radium by the manganese and iron oxides. They provided the basis for further analyzing the distribution of radium isotopes.

5.1.3 Effect of cation exchange capacity

The exchange of similar cations can elevate the concentration of radium isotopes desorbed in water with high salinity or TDS (Szabo et al., 2012; Tang et al., 2015). As described in the previous studies, the exchange between the ions of Na^+, Mg^{2+}, and Ca^{2+} prevented the decay of radium isotopes. Therefore, the activity of radium isotope in water with divalent cations was generally higher than that in water with

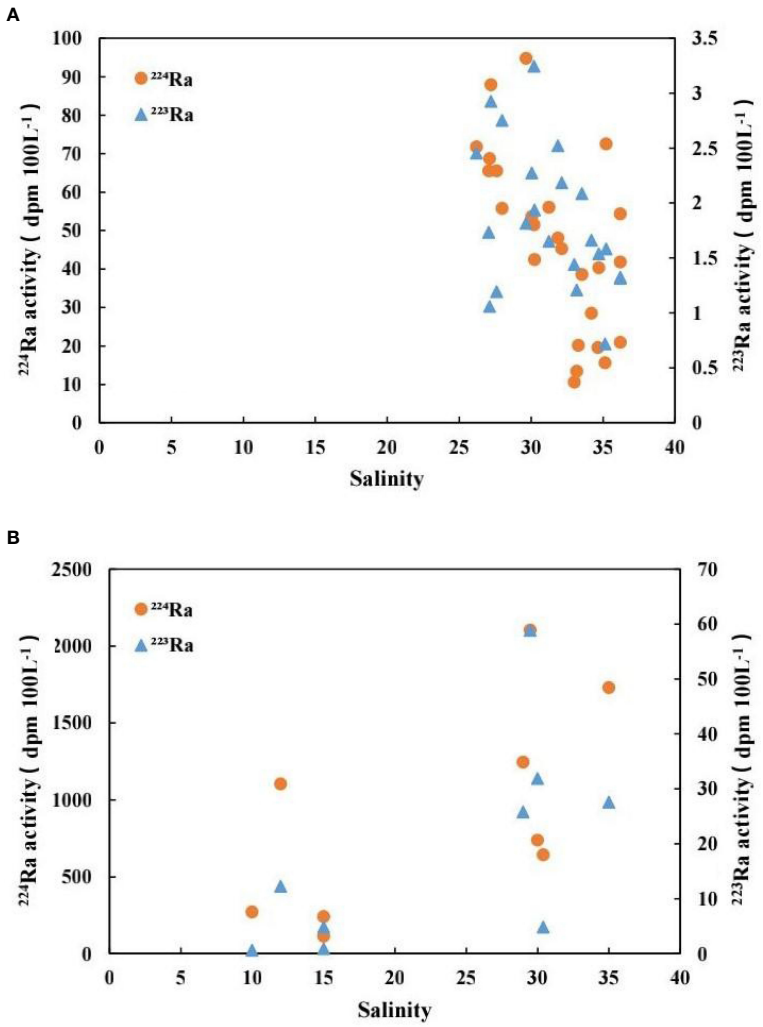

FIGURE 6
The relationship between radium isotope activity and salinity in water: **(A)** ^{223}Ra and ^{224}Ra in seawater change with salinity; **(B)** ^{223}Ra and ^{224}Ra in groundwater change with salinity.

monovalent cations as the main components (Vinson et al., 2013). Figures 7C, D show the variation of the ratios of cations of Ca^{2+}/Na^{+} and Mg^{2+}/Na^{+} in seawater with ^{223}Ra and ^{224}Ra activities. The activities of ^{224}Ra have positively correlated with Ca^{2+}/Na^{+} and Mg^{2+}/Na^{+} generally; however, there was only a slight correlation between the activities of ^{223}Ra and Ca^{2+}/Na^{+} and Mg^{2+}/Na^{+}. It indicated that the exchange ability of ions with the same valence in water increased when the relative ion concentration of Ca^{2+} and Mg^{2+} increased. As a result, more radium isotopes were dissolved and the decay of radium isotopes was inhibited indirectly. Therefore, more dissolved radium isotopes can be measured in the water. Due to the experimental error and the influence of human factors, the relationship between ^{223}Ra and Ca^{2+}/Na^{+} and Mg^{2+}/Na^{+} was not obvious.

5.2 Estimation of SGD fluxes

5.2.1 River input and sediment diffusion input

During the sampling period, no water samples from the Shahe River were taken because the lower reach of the Shahe River dried up. Therefore, the radium activity in the Shahe River was ignored. The cumulative radium flux input into the river of the study area was calculated by obtaining the flow data of each river except the Shahe River. ^{224}Ra on the particulate matter of the river in the estuarine area was rapidly desorbed due to the increase in water concentration. The radium activity in the estuarine area was higher than that in the middle–upper section of the river. The concentration of ^{224}Ra activity in the estuary area was selected to calculate the quantity of ^{224}Ra, which was more representative of the river input into the seawater. The

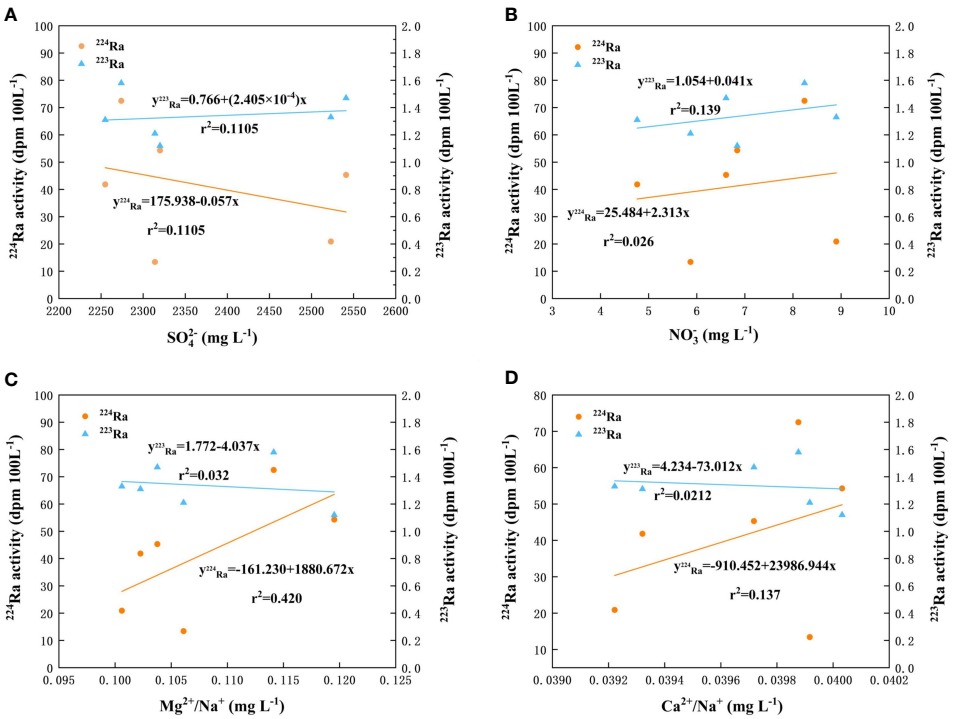

FIGURE 7
The relationship diagram between ^{223}Ra and ^{224}Ra and SO_4^{2-} **(A)**, NO_3^- **(B)**, Mg^{2+}/Na^+ **(C)**, and Ca^{2+}/Na^+ **(D)** in seawater.

calculated value of ^{224}Ra input from the rivers in the study area was 2.76 × 10^9 dpm day^{-1} in September 2019 based on Eq. (4).

Moore (2007) concluded that the diffusion flux of ^{224}Ra in the fine-grained sediments was about 210 dpm/m^2/100 L. The area of the seafloor sediments in the study area was about 1,750 km^2, and the diffused amount of ^{224}Ra in the seabed sediments was about 3.67 × 10^{11} dpm day^{-1} based on Eq. (5).

5.2.2 Mixed loss and decay

The inventory of ^{224}Ra in the study area $V_{bay}{}^{224}Ra_{bay}V_{bay}{}^{224}Ra_{bay}$ was obtained based on the water depth and ^{224}Ra activity of the seawater sampling points. The sea area was divided into 48 triangular elements based on the sampling points. The inventory of ^{224}Ra was calculated by multiplying the area, the average water depth, and the average ^{224}Ra activity in each triangular element. Finally, the inventory of ^{224}Ra in the study area was calculated by adding the inventory of ^{224}Ra in each triangular element.

The background value of seawater outside the studied sea area was 15.72 dpm $100L^{-1}$, which was the average value of SW22 and SW23. The reason was that the radium active values of SW22 and SW23 were the lowest ones at the sampling locations near the open sea (Peterson et al., 2008). The diffusion value of ^{224}Ra was about 3.20 × 10^{11} dpm day^{-1} based on Eq. (6). The loss term caused by the radioactive decay of ^{224}Ra was about 1.17 × 10^{12} dpm day^{-1} based on Eq. (7).

5.2.3 Estimating the SGD flux

With regard to the value of $^{224}Ra_{GW}$, the radium ^{224}Ra in the nearshore groundwater was more representative of the groundwater input into the seawater. Therefore, the average activity of ^{224}Ra in coastal groundwater (the average value after removing the abnormally high value and low value) was selected as the end value of groundwater.

The ^{224}Ra fluxes obtained by calculation and the relevant parameters are reported in Table 4. Substituting the obtained ^{224}Ra fluxes from rivers F_{river}, from diffusion of seabed sediments F_{sed}, from radioactive decay F_{decay}, and from mixed diffusion F_{mixing} into Eq. (3), the value of F_{SGD} based on the balance model of radium mass was estimated to be 1.12 × 10^{12} dpm day^{-1}. Among the source items, the ^{224}Ra fluxes from the river input accounted for the smallest proportion, and the ^{224}Ra fluxes from decay loss accounted for the largest proportion among the sink items (Table 4). Finally, the total average SGD fluxes were about 1.31 × 10^8 m^3 day^{-1} based on Eq. (8), and the average SGD rate was 7.49 cm day^{-1}. Compared with the SGD flux in other bays of China by other investigators as summarized in Table 5, the SGD rate of this

TABLE 4 The values of the parameters used in the model of radium mass balance.

Parameters	Values	Unit
V_{bay}	1.31×10^{10}	m^3
A_{sed}	1.75×10^{9}	m^2
T_f	13.0	day
$^{224}Ra_{bay}$	47.32	dpm 100 L^{-1}
$^{224}Ra_{sea}$	15.72	dpm 100 L^{-1}
$^{224}Ra_{GW}$	852.86	dpm 100 L^{-1}
F_{river}	2.76×10^{9}	dpm day^{-1}
F_{decay}	1.17×10^{12}	dpm day^{-1}
F_{sed}	3.67×10^{11}	dpm day^{-1}
F_{mixing}	3.20×10^{11}	dpm day^{-1}
F_{SGD}	1.12×10^{12}	dpm day^{-1}
V_{SGD}	1.31×10^{8}	m^3 day^{-1}

study area was in the middle value. Additionally, the estimated SGD in this study area may be larger because the suspended particulate matter desorption was not measured directly.

5.3 Correlation analysis and SGD-derived nutrient fluxes

The quantification of SGD flux was important for environmental governance because the SGD was the main pollution source. The pollution problem has increased seriously in eastern Liaodong Bay in recent years. For example, the problem of eutrophication happened in the local water. The SGD-derived nutrient flux was calculated by multiplying the SGD flux and the nutrient concentration in the groundwater terminal member. Generally, the concentration of nutrients refers to the average concentration at each end-member. The nutrient fluxes carried by the river could be determined by the discharge rates in the river water and the related nutrient concentrations. The calculation formula of the nutrients driven by the SGD or river was as follows:

$$F_m = V_{SGD} M_x \quad , \quad (9)$$

where F_m is the flux of nutrients from the SGD or river and M_x is the concentration of nutrients in groundwater or river water.

As shown in Figure 8, the SGD-derived nutrients were 7.16×10^7 mol day^{-1} for DIN, 1.01×10^6 mol day^{-1} for DIP, 1.61×10^7 mol day^{-1} for NH_4^+, 0.92×10^6 mol day^{-1} for NO_2^-, and 5.41×10^7 mol day^{-1} for NO_3^-. The nutrient fluxes carried by the river were 3.44×10^6 mol day^{-1} for DIN, 3.90×10^4 mol day^{-1} for DIP, 3.78×10^5 mol day^{-1} for NH_4^+, 1.52×10^4 mol day^{-1} for NO_2^-, and 3.01×10^6 mol day^{-1} for NO_3^-. The results indicated that the nutrient fluxes carried by the SGD were much higher than those from river inputs. For instance, the SGD-derived nutrient fluxes of DIN were 90–131 times higher than those of rivers, and the SGD was the main channel to carry the source of nutrients into the sea area. The impact of SGD on the coastal zone and marine ecosystem in eastern Liaodong Bay was greater than that of rivers.

5.4 Uncertainty analysis

In the radium mass balance model, some items have great uncertainties. The uncertainties may be related to the selection of the groundwater end-member value, the river flow, and the inventory of radium. The groundwater end-member value was one of the key factors for the uncertainty of estimation results

TABLE 5 Comparison of the results of SGD flux in different study areas.

Site	Method	SGD flux (cm day^{-1})	Study area (m^2)	Author
Tolu Bay, China	^{223}Ra, ^{224}Ra	7.5–20	8×10^6	Luo et al. (2014)
Laizhou Bay, China	^{223}Ra, ^{226}Ra	8.86–11.33	6×10^9	Wang et al. (2015)
Jiaozhou Bay, China	^{223}Ra, ^{224}Ra	4.98–6.3	2.97×10^8	Zhang et al. (2020b)
Daya Bay, China	^{223}Ra, ^{224}Ra, ^{226}Ra, ^{228}Ra	6.0–8.6	5.56×10^8	Zhang et al. (2020c)
Bohai Bay, China	^{223}Ra, ^{228}Ra	1.5–8.8	1.61×10^{10}	Wang et al. (2019)
Liaodong Bay, China	^{223}Ra, ^{224}Ra	7.49	1.75×10^9	This study

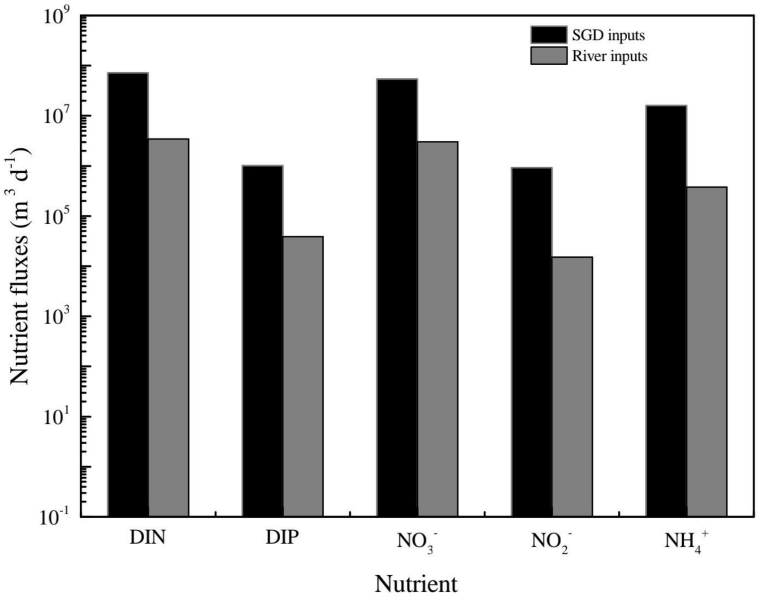

FIGURE 8
The nutrient fluxes from the SGD and river.

(Peterson et al., 2008; Xu et al., 2013). The SGD flux obtained will decrease by about 50% if the maximum value of ^{224}Ra activity in groundwater (to remove the abnormally high value and low value) was selected for the calculation. Previous studies suggested that the uncertainty of model estimation will be reduced by increasing the number of groundwater samples (Wang et al., 2020b). The SGD fluxes will increase or decrease by about 1% if the average river flow is increased or decreased by 50%, which indicated that the quantity of river flow had a little effect on SGD fluxes. Thus, SGD fluxes should be estimated thoroughly based on the actual conditions.

6 Conclusions

Based on analyzing the radium activities of ^{223}Ra and ^{224}Ra in eastern Liaodong Bay, it was concluded that the distribution of short-lived radium isotopes was influenced by the water body type and geochemical factors. In general, the radium concentrations of groundwater were much greater than those in the bay, and in the south, they were larger than those in the north as a whole. The relationship between radium and chemical composition was analyzed. Radium has a negative correlation with salinity and sulfate concentration. However, radium was positively correlated to the concentrations of cations Ca^{2+} and Mg^{2+}. The average apparent water age was calculated to be 13.0 days, and the average SGD flux was determined to be 1.31×10^8 m^3/day based on the ^{224}Ra model of mass balance. In addition, the ratio of DIN to DIP in the water body of Liaodong Bay was higher, and the SGD-derived nutrient fluxes were estimated to be 7.16×10^7 mol day^{-1} for DIN, 1.01×10^6 mol day^{-1} for DIP, 1.61×10^7 mol day^{-1} for NH_4^+, 0.92×10^6 mol day^{-1} for NO_2^-, and 5.41×10^7 mol day^{-1} for NO_3^-. The nutrient fluxes from riverine inputs were much lower than those from the SGD. The SGD played a decisive role in changing the ecosystem of seawater. The water body in eastern Liaodong Bay was in a state of eutrophication. The nutrient fluxes carried by the SGD should be given attention for the protection and preservation of the environment and the prevention of water pollution.

Data availability statement

The original contributions presented in the study are included in the article/supplementary material. Further inquiries can be directed to the corresponding author.

Author contributions

QG: methodology and writing and preparation of the original draft. YZ, ML, and JL: investigation and data analysis. All authors contributed to the article and approved the submitted version.

Funding

This work was supported by the National Natural Science Foundation of China (Grant No. 41772235) and the

Fundamental Research Funds for the Central Universities (No. B210202108).

Conflict of interest

The authors declare that the research was conducted in the absence of any commercial or financial relationships that could be construed as a potential conflict of interest.

Publisher's note

All claims expressed in this article are solely those of the authors and do not necessarily represent those of their affiliated organizations, or those of the publisher, the editors and the reviewers. Any product that may be evaluated in this article, or claim that may be made by its manufacturer, is not guaranteed or endorsed by the publisher.

References

Beck, A. J., Rapaglia, J. P., Cochran, J. K., and Bokuniewicz, H. J. (2007). Radium mass-balance in Jamaica bay, NY: Evidence for a substantial flux of submarine groundwater. *Mar. Chem.* 106, 419–441. doi: 10.1016/j.marchem.2007.03.008

Burnett, W. C., Aggarwal, P. K., Aureli, A., Bokuniewicz, H., Cable, J. E., Charette, M. A., et al. (2006). Quantifying submarine groundwater discharge in the coastal zone *via* multiple methods. *Sci. Total Environ.* 367 (2-3), 498–543. doi: 10.1016/j.scitotenv.2006.05.009

Burnett, W. C., Bokuniewicz, H., Huettel, M., Moore, W. S., and Taniguchi, M. (2003). Groundwater and pore water inputs to the coastal zone. *Biogeochemistry* 66, 3–33. doi: 10.1023/B:BIOG.0000006066.21240.53

Burt, W. J., Thomas, H., and Auclair, J. P. (2013). Short-lived radium isotopes on the scotian shelf: unique distribution and tracers of cross-shelf CO_2 and nutrient transport. *Mar. Chem.* 156, 120–129. doi: 10.1016/j.marchem.2013.05.007

Cai, W., Meng, W., Zhu, Y., Zhou, J., and Liu, L. (2013). Assessing benthic ecological status in stressed liaodong bay (China) with AMBI and m-AMBI. *Chin. J. Oceanol. Limnol.* 31, 482–492. doi: 10.1007/s00343-013-2177-0

Charette, M. A., Splivallo, R., Herbold, C., Bollinger, M. S., and Moore, W. S. (2003). Salt marsh submarine groundwater discharge as traced by radium isotopes. *Mar. Chem.* 84, 113–121. doi: 10.1016/j.marchem.2003.07.001

Cho, H., Kim, G., Kwon, E., Moosdorf, N., Garcia-Orellana, J., and Santos, I. (2018). Radium tracing nutrient inputs through submarine groundwater discharge in the global ocean. *Sci. Rep.* 8, 2439. doi: 10.1038/s41598-018-20806-2

Debnath, P., and Mukherjee, A. (2016). Quantification of tidally-influenced seasonal groundwater discharge to the bay of Bengal by seepage meter study. *J. Hydrol.* 537, 106–116. doi: 10.1016/j.jhydrol.2016.03.010

Dulaiova, H., and Burnett, W. C. (2008). Evaluation of the flushing rates of Apalachicola bay, Florida *via* natural geochemical tracers. *Mar. Chem.* 109, 395–408. doi: 10.1016/j.marchem.2007.09.001

Ganguli, P. M., Conaway, C. H., Swarzenski, P. W., Izbicki, J. A., and Flegal, A. R. (2012). Mercury speciation and transport *via* submarine groundwater discharge at a southern California coastal lagoon system. *Environ. Sci. Technol.* 46 (3), 1480–1488. doi: 10.1021/es202783u

Gonneea, M. E., Morris, P. J., Dulaiova, H., and Charette, M. A. (2008). New perspectives on radium behavior within a subterranean estuary. *Mar. Chem.* 109 (3-4), 250–267. doi: 10.1016/j.marchem.2007.12.002

Gopinath, S., Srinivasamoorthy, K., Saravanan, K., Prakash, R., and Karunanidhi, D. (2019). Characterizing groundwater quality and seawater intrusion in coastal aquifers of nagapattinam and karaikal, south India using hydrogeochemistry and modeling techniques. *Hum. Ecol. Risk Assess. Int. J.* 25 (1-2), 314–334. doi: 10.1080/10807039.2019.1578947

Gopinath, S., Srinivasamoorthy, K., Saravanan, K., Suma, C. S., Prakash, R., Senthilnathan, D., et al. (2016). Modeling saline water intrusion in nagapattinam coastal aquifers, tamilnadu, India. *Model. Earth Syst. Environ.* 2 (2), 1–10. doi: 10.1007/s40808-015-0058-6

Guo, Q. N., and Li, H. L. (2015). Terrestrial-originated submarine groundwater discharge through deep multilayered aquifer systems beneath the seafloor. *Hydrol. Process.* 29 (2), 295–309. doi: 10.1002/hyp.10163

Guo, Y. D., Mei, X., Meng, X. J., Lan, X. H., Chen, H. J., and Yang, H. (2020b). Benthic foraminifera and its response to heavy metal pollution: A case study from liaodong bay, China. *Mar. pollut. Bull.* 154, 111084. doi: 10.1016/j.marpolbul.2020.111084

Guo, Q. N., Zhang, J. M., Hu, Z. L., and Zhou, Z. W. (2020a). Hydrochemical evolution of groundwater in coastal plain area of the downstream of daqing river, liaodong bay, china. J. *Coast. Res.* 36 (3), 608–618. doi: 10.2112/JCOASTRES-D-19-00114.1

Hwang, D. W., Lee, I. S., Choi, M., and Kim, T. H. (2016). Estimating the input of submarine groundwater discharge (SGD) and SGD-derived nutrients in geoje bay, Korea using ^{222}Rn-Si mass balance model. *Mar. pollut. Bull.* 110 (1), 119–126. doi: 10.1016/j.marpolbul.2016.06.073

Kim, I., and Kim, G. (2011). Large Fluxes of rare earth elements through submarine groundwater discharge (SGD) from a volcanic island, jeju, Korea. *Mar. Chem.* 127 (1-4), 12–19. doi: 10.1016/j.marchem.2011.07.006

Kim, G., Ryu, J. W., Yang, H. S., and Yun, S. T. (2005). Submarine groundwater discharge (SGD) into the yellow Sea revealed by Ra-228 and Ra-226 isotopes: implications for global silicate fluxes. *Earth Planet. Sci. Lett.* 237 (1-2), 156–166. doi: 10.1016/j.epsl.2005.06.011

Lamontagne, S., Taylor, A. R., Herpich, D., and Hancock, G. J. (2015). Submarine groundwater discharge from the south Australian limestone coast region estimated using radium and salinity. *J. Environ. Radioact.* 140, 30–41. doi: 10.1016/j.jenvrad.2014.10.013

Lan, X., Meng, X., Mei, X., Xu, Y., Huang, L., and Chen, S. (2018). Pollution characteristics and quality assessment of heavy metals in surface sediments from the liaodong bay. *Acta Oceanologica Sin.* 40, 60–73 (In Chinese with English abstract).

Lee, C. M., Jiao, J. J., Luo, X., and Moore, W. S. (2012). Estimation of submarine groundwater discharge and associated nutrient fluxes in tolo harbour, Hong Kong. *Sci. Total Environ.* 433, 427–433. doi: 10.1016/j.scitotenv.2012.06.073

Li, X. J., Chen, L. L., Zhou, Z. Q., Li, B. Q., Liu, X., Yang, L. F., et al. (2019). Spatio-temporal variation of subtidal macrobenthic fauna and the ecological assessment of longkou artificial island construction in bohai Sea, China. *J.Oceanol.Limnol.* 38 (6), 1811–1824. doi: 10.1007/s00343-019-9098-5

Lignell, R., Hoikkala, L., and Lahtinen, T. (2008). Effects of inorganic nutrients, glucose and solar radiation on bacterial growth and exploitation of dissolved organic carbon and nitrogen in the northern Baltic Sea. *Aquat. Microb. Ecol.* 51 (3), 209–221. doi: 10.3354/ame01202

Li, X. Z., Lei, G. C., Li, Y. L., Wang, Y. Y., and Tan, Z. Q. (2021). Assessing hydrodynamic effects of ecological restoration scenarios for a tidal-dominated wetland in liaodong bay. *Sci. Total Environ.* 752, 142339. doi: 10.1016/j.scitotenv.2020.142339

Liu, J., Du, J., and Yi, L. (2017). Ra Tracer-based study of submarine groundwater discharge and associated nutrient fluxes into the bohai Sea, China: a highly human-affected marginal sea. *J. Geophys. Res. Oceans* 122, 8646–8660. doi: 10.1002/2017JC013095

Liu, Y., Jiao, J. J., Mao, R., Luo, X., Liang, W., and Robinson, C. E. (2019). Spatial characteristics reveal the reactive transport of radium isotopes (224Ra, 223Ra, and 228Ra) in an intertidal aquifer. *Water Resour. Res.* 55 (12), 10282–10302. doi: 10.1029/2019WR024849

Liu, L., Yi, L., Cheng, X., and Tang, G. (2015). Distribution of (223)Ra and (224) Ra in the bo Sea embayment in tianjin and its implication of submarine groundwater discharge. *J. Environ. Radioactiv.* 150, 111–120. doi: 10.1016/j.jenvrad.2015.08.008

Li, H. L., and Wang, X. J. (2015). Review and progress of the study on submarine groundwater discharge. *Adv. Earth Sci.* 30 (06), 636–646. (In Chinese).

Lopez, C. V., Murgulet, D., and Santos, I. R. (2020). Radioactive and stable isotope measurements reveal saline submarine groundwater discharge in a semiarid estuary. *J. Hydrol.* 590, 125395. doi: 10.1016/j.jhydrol.2020.125395

Luo, X., and Jiao, J. J. (2016). Submarine groundwater discharge and nutrient loadings in tolo harbor, Hong Kong using multiple geotracer-based models, and their implications of red tide outbreaks. *Water Res.* 102, 11–31. doi: 10.1016/j.watres.2016.06.017

Luo, X., Jiao, J. J., Moore, W. S., and Lee, C. M. (2014). Submarine groundwater discharge estimation in an urbanized embayment in Hong Kong *via* short-lived radium isotopes and its implication of nutrient loadings and primary production. *Mar. pollut. Bull.* 82 (1-2), 144–154. doi: 10.1016/j.marpolbul.2014.03.005

Makings, U., Santos, I. R., Maher, D. T., Golsby-Smith, L., and Eyre, B. D. (2014). Importance of budgets for estimating the input of groundwater derived nutrients to an eutrophic tidal river and estuary. *Estuar. Coast. Shelf Sci.* 143, 65–76. doi: 10.1016/j.ecss.2014.02.003

Ma, D., and Wang, J. (2003). Evaluation on potential ecological risk of sediment pollution in main estuaries of China. *China Environ. Sci.* 23, 521–525. (In Chinese).

Ma, J., Zhou, Z., Guo, Q., Zhu, S., Dai, Y., and Shen, Q. (2019). *Spatial characterization of seawater intrusion in a coastal aquifer of northeast liaodong bay, China* (7013: Sustainability.11). doi: 10.3390/su11247013

Moore, W. S. (1996). Large Groundwater inputs to coastal waters revealed by ^{226}Ra enrichments. *Nature.* 380, 612–614. doi: 10.1038/380612a0

Moore, W. S. (1999). The subterranean estuary: a reaction zone of ground water and sea water. *Mar. Chem.* 65, 111–125. doi: 10.1016/S0304-4203(99)00014-6

Moore, W. S. (2000). Ages of continental shelf waters determined from ^{223}Ra and ^{224}Ra. *J. Geophys. Res. Oceans* 105 (C9), 22117–22122. doi: 10.1029/1999JC000289

Moore, W. S. (2007). Seasonal distribution and flux of radium isotopes on the southeastern US continental shelf. *J. Geophys. Res. Oceans* 112 (C10), C10013. doi: 10.1029/2007JC004199

Moore, W. S. (2008). Fifteen years experience in measuring ^{224}Ra and ^{223}Ra by delayed-coincidence counting. *Mar. Chem.* 109, 188–197. doi: 10.1016/j.marchem.2007.06.015

Moore, W. S., Blanton, J. O., and Joye, S. B. (2006). Estimates of apparent water ages, submarine groundwater discharge, and nutrient fluxes to okatee estuary, south Carolina. *J. Geophys. Res. Oceans* 111 (C9), C09006. doi: 10.1029/2005JC003041

Moore, W. S., and Krest, J. (2004). Distribution of ^{223}Ra and ^{224}Ra in the plumes of the Mississippi and atchafalaya rivers and the gulf of Mexico. *Mar. Chem.* 86, 105–119. doi: 10.1016/j.marchem.2003.10.001

Moore, W. S., and Reid, D. F. (1973). Extraction of radium from natural waters using manganese impregnated acrylic fibers. *J. Geophys. Res. Oceans.* 78, 8880–8886. doi: 10.1029/JC078i036p08880

Pei, S. F., Laws, E. A., Zhu, Y. X., Zhang, H. B., Ye, S. Y., Yuan, H. M., et al. (2019). Nutrient dynamics and their interaction with phytoplankton growth during autumn in liaodong bay, China. *Cont. Shelf Res.* 186, 34–47. doi: 10.1016/j.csr.2019.07.012

Peng, S. (2015). The nutrient, total petroleum hydrocarbon and heavy metal contents in the seawater of bohai bay, China: temporal-spatial variations, sources, pollution statuses, and ecological risks. *Mar. pollut. Bull.* 95, 445–451. doi: 10.1016/j.marpolbul.2015.03.032

Peterson, R. N., Burnett, W. C., Taniguchi, M., Chen, J., Santos, I. R., and Misra, S. (2008). Determination of transport rates in the yellow river-bohai Sea mixing zone *via* natural geochemical tracers. *Cont. Shelf Res.* 28 (19), 2700–2707. doi: 10.1016/j.csr.2008.09.002

Prakash, R., Srinivasamoorthy, K., Gopinath, S., and Saravanan, K. (2018). Measurement of submarine groundwater discharge using diverse methods in coleroon estuary, Tamil nadu, India. *Appl. Water Sci.* 8 (13), 1–13. doi: 10.1007/s13201-018-0659-0

Prakash, R., Srinivasamoorthy, K., Gopinath, S., and Saravanan, K. (2020). Submarine groundwater discharge as sources for dissolved nutrient fluxes in coleroon river estuary, bay of Bengal, India. *J. Contam. Hydrol.* 233, 103660. doi: 10.1016/j.jconhyd.2020.103660

Qiao, Y., Feng, J., Cui, S., and Zhu, L. (2017). Long-term changes in nutrients, chlorophylla and their relationships in a semi-enclosed eutrophic ecosystem, bohai bay, China. *Mar. pollut. Bull.* 117, 222–228. doi: 10.1016/j.marpolbul.2017.02.002

Refiled, A. C., Ketchum, B. H., and Rechards, F. A. (1963). The influence of organisms on the composition of seawater. *sea* 2, 66–77.

Santos, I. R., Chen, X., Lecher, A. L., Sawyer, A. H., Moosdorf, N., Rodellas, V., et al. (2021). Submarine groundwater discharge impacts on coastal nutrient biogeochemistry. *Nat. Rev. Earth Environ.* 2, 307–323. doi: 10.1038/s43017-021-00152-0

Slomp, C. P., and Van Cappellen, P. (2004). Nutrient inputs to the coastal ocean through submarine groundwater discharge: controls and potential impact. *J.Hydrol.* 295 (1-4), 64–86. doi: 10.1016/j.jhydrol.2004.02.018

Song, J., and Duan, L. (2019). "Chapter 17-the bohai Sea," in *World seas: An environmental evaluation, second edition*. Ed. C. Sheppard Elsevier, 377–394. doi: 10.1016/B978-0-08-100853-9.00024-5

Swarzenski, P., Baskaran, M., Rosenbauer, R., Edwards, B., and Land, M. (2013). A combined radio- and stable-isotopic study of a California coastal aquifer system. *Water* 5 (2), 480–504. doi: 10.3390/w5020480

Szabo, Z., Vincent, T., Fischer, J. M., Kraemer, T. F., and Jacobsen, E. (2012). Occurrence and geochemistry of radium in water from principal drinking-water aquifer systems of the united states. *Appl. Geochem.* 27 (3), 729–752. doi: 10.1016/j.apgeochem.2011.11.002

Tang, G., Yi, L., Liu, L., and Cheng, X. (2015). Factors influencing the distribution of ^{223} Ra and ^{224}Ra in the coastal waters off tanggu and qikou in bohai bay. *Cont. Shelf Res.* 109, 177–187. doi: 10.1016/j.csr.2015.09.003

Taniguchi, M., Burnett, W. C., Cable, J. E., and Turner, J. V. (2002). Investigation of submarine groundwater discharge. *Hydrol. Process.* 16, 2115–2129. doi: 10.1002/hyp.1145

Taniguchi, M., Dulai, H., Burnett, K. M., Santos, I. R., Sugimoto, R., Stieglitz, T., et al. (2019). Submarine groundwater discharge: updates on its measurement techniques, geophysical drivers, magnitudes, and effects. *Front. Environ. Sci.* 7. doi: 10.3389/fenvs.2019.00141

TSGSBOLP (The Seventh Geological Survey Brigade of Liaoning Province) (1973). *The survery report of daqing river lower vally plain; hydrographic service: Liaoning, China*.

Vaeret, L., Leijnse, A., Cuamba, F., and Haldorsen, S. (2012). Holocene Dynamics of the salt–fresh groundwater interface under a sand island, inhaca, Mozambique. *Quat. Int.* 257, 74–82. doi: 10.1016/j.quaint.2011.11.020

Vinson, D. S., Tagma, T., Bouchaou, L., Dwyer, G. S., Warner, N. R., and Vengosh, A. (2013). Occurrence and mobilization of radium in fresh to saline coastal groundwater inferred from geochemical and isotopic tracers (Sr, s, O, h, Ra, Rn). *Appl. Geochem.* 38, 161–175. doi: 10.1016/j.apgeochem.2013.09.004

Wang, X. L., Cui, Z. G., Guo, Q., Han, X. R., and Wang, J. T. (2009). Distribution of nutrients and eutrophication assessment in the bohai Sea of China. *Chin. J. Oceanol. Limnol.* 27, 177–183. doi: 10.1007/s00343-009-0177-x

Wang, X. J., Li, H. L., Jiao, J. J., Barry, D. A., Li, L., Luo, X., et al. (2015). Submarine fresh groundwater discharge into laizhou bay comparable to the yellow river flux. *Sci. Rep.* 5, 8814. doi: 10.1038/srep08814

Wang, X. J., Li, H. L., Luo, X., Jiao, J. J., Qu, W. J., and and Wang, C. Y (2016). Using ^{224}Ra to estimate eddy diffusivity and submarine groundwater discharge in Laizhou bay, China. *J. Radioanal. Nucl. Chem.* 308, 403–41. doi: 10.1007/s10967-015-4495-5

Wang, Q. Q., Li, H. L., Zhang, Y., Wang, X. J., Xiao, K., Zhang, X. L., et al. (2020b). Submarine groundwater discharge and its implication for nutrient budgets in the western bohai bay, China. *J. Environ. Radioactiv.* 212, 106132. doi: 10.1016/j.jenvrad.2019.106132

Wang, Q. Q., Li, H. L., Zhang, Y., Wang, X. J., Zhang, C. C., Xiao, K., et al. (2019). Evaluations of submarine groundwater discharge and associated heavy metal fluxes in bohai bay, China. *Sci. Total Environ.* 695, 133873. doi: 10.1016/j.scitotenv.2019.133873

Wang, X. J., Li, H. L., Zhang, Y., Zheng, C. M., and Gao, M. S. (2020c). Investigation of submarine groundwater discharge and associated nutrient inputs into laizhou bay (China) using radium quartet. *Mar. pollut. Bull.* 157, 111359. doi: 10.1016/j.marpolbul.2020.111359

Wang, X. J., Li, H. L., Zheng, C. M., Yang, J. Z., Zhang, Y., Zhang, M., et al. (2018). Submarine groundwater discharge as an important nutrient source influencing nutrient structure in coastal water of daya bay, China. *Geochim. Cosmochim. Acta* 225, 52–65. doi: 10.1016/j.gca.2018.01.029

Wang, X. F., Wei, F. S., and Qi, W. Q. (2002). *Water and wastewater monitoring and analysis methods (fourth ed.)* (Beijing, China: Environmental Science Press). (in Chinese).

Wang, P., Zhang, L. J., Lin, X., Yan, J. S., Zhang, P., Zhao, B., et al. (2020a). Spatial distribution, control factors and sources of heavy metal in the surface sediments of fudu estuary waters, East liaodong bay, China. *Mar. pollut. Bull.* 156, 111279. doi: 10.1016/j.marpolbul.2020.111279

Webster, I. T., Hancock, G. J., and Murray, A. S. (1995). Modelling the effect of salinity on radium desorption from sediments. *Geochem. Cosmochim. Acta* 59 (12), 2469–2476. doi: 10.1016/0016-7037(95)00141-7

Xiao, K., Li, G., Li, H. L., Zhang, Y., Wang, X. J., Hu, W. L., et al. (2019). Combining hydrological investigations and radium isotopes to understand the environmental effect of groundwater discharge to a typical urbanized estuary in China. *Sci. Total Environ.* 695, 133872. doi: 10.1016/j.scitotenv.2019.133872

Xiong, W., Mei, X., Meng, X. J., Chen, H. J., and Yang, H. (2020). Phytoplankton biomarkers in surface sediments from liaodong bay and their potential as indicators of primary productivity. *Mar. pollut. Bull.* 159, 111536. doi: 10.1016/j.marpolbul.2020.111536

Xu, B., Burnett, W., Dimova, N., Diao, S., Mi, T., Jiang, X., et al. (2013). Hydrodynamics in the yellow river estuary *via* radium isotopes: ecological perspectives. *Cont. Shelf Res.* 66, 19–28. doi: 10.1016/j.csr.2013.06.018

Ye, S., Laws, E. A., Yuknis, N., Ding, X., Yuan, H., Zhao, G., et al. (2015). Carbon sequestration and soil accretion in coastal wetland communities of the yellow river delta and liaohe delta, China. *Estuar. Coasts* 38, 1885–1897. doi: 10.1007/s12237-014-9927-x

Zhang, Y., Li, H. L., Wang, X. J., Zheng, C. M., Wang, C. Y., Xiao, K., et al. (2016). Estimation of submarine groundwater discharge and associated nutrient fluxes in eastern laizhou bay, China using ^{222}Rn. *J. Hydrol.* 533, 103–113. doi: 10.1016/j.jhydrol.2015.11.027

Zhang, Y., Li, H. L., Xiao, K., Wang, X. J., Lu, X. T., Zhang, M., et al. (2017). Improving estimation of submarine groundwater discharge using radium and radon tracers: application in jiaozhou bay, China. *J. Geophys. Res.Oceans* 122 (10), 8263–8277. doi: 10.1002/2017jc013237

Zhang, Y., Santos, I. R., Li, H., Wang, Q., Xiao, K., Guo, H., et al. (2020a). Submarine groundwater discharge drives coastal water quality and nutrient budgets at small and large scales. *Geochim. Cosmochim. Acta* 290, 201–215. doi: 10.1016/j.gca.2020.08.026

Zhang, Y., Wang, X., Li, H., and Song, D. (2020b). Large inputs of groundwater and associated fluxes of alkalinity and nutrients into Jiaozhou Bay, China. *Hydrogeol. J* 28, 1721–1734. doi: 10.1007/s10040-020-02144-8

Zhang, Y., Li, H., Zheng, C., Wang, X., Shang, M., and Xiao, K. (2020c). Improvement of evaluation of water age and submarine groundwater discharge: A case study in Daya Bay,China. *J Hydrol*. 586, 124775. doi: 10.1016/j.jhydrol.2020.124775

Zhu, S. M., Zhou, Z. F., Guo, Q. N., and Ma, J. (2020). A study on the cause of layered seawater intrusion in the daqing river estuary of liaodong bay, China. *Sustainability* 12 (7), 2842. doi: 10.3390/su12072842